Carbonate weathering-related carbon sink fluxes under different land uses: A case study from the Shawan Simulation Test Site, Puding, Southwest China

Qingrui Zeng[a,b,c], Zaihua Liu[a,c,*], Bo Chen[a,b,c], Yundi Hu[a,b,c], Sibo Zeng[d], Cheng Zeng[a,c], Rui Yang[a], Haibo He[a,b], Hui Zhu[a,c], Xianli Cai[c], Jia Chen[c], Yi Ou[c]

[a] State Key Laboratory of Environmental Geochemistry, Institute of Geochemistry, CAS, Guiyang 550081, China
[b] University of Chinese Academy of Sciences, Beijing 100049, China
[c] Puding Karst Ecosystem Research Station, CAS, Puding 562100, China
[d] School of Geographical Sciences, Southwest University, Chongqing 400715, China

A R T I C L E   I N F O

A B S T R A C T

In the study of global climate change, a major focus of research into the carbon cycle is to determine the fate of missing carbon sinks. Carbonate weathering-related carbon sinks as a result of water-carbonate-CO_2-aquatic phototroph interactions may make a major contribution. Establishing optimal land uses, which determine soil CO_2 concentrations and water supplies for carbonate dissolution, may be a feasible and effective way to increase the sink potential. Elucidating both the hydrological and the hydrochemical behavior under different land uses is critical for rational planning of land use changes to increase the carbon sink. Given the complexity within natural karst catchments, the Shawan Simulation Test Site was established at Puding, Southwest China, to simulate the influence of land uses with controlled carbonate test beds - bare rock, bare soil, crop land, grass land, shrub land. Soil CO_2 concentrations, hydrochemical parameters (pH, major ion concentrations) and the 'spring' (artificial drain) discharge were intensively measured from Sept. 1, 2015 to Aug. 31, 2016 to investigate the carbon and water responses to different land uses in different seasons. In the vegetated land uses (crop, grass or shrub), DIC increased due to the increase of soil CO_2 resulting from stronger microbial activities and root respiration in summer and autumn growing seasons. In the bare rock and soil cases, there was also an increase in DIC in summer and autumn, due to decomposition of prior organic matter within soils and/or rock pores. The average DIC concentration ranking, high to low, was grass land, shrub land, crop land, bare soil, bare rock. Soil CO_2 concentration was thus the dominant of DIC concentration, which is a key multiplier of carbon sink fluxes ($CSF = 0.5 * [DIC] * RD$, where RD is depth of runoff, [DIC] is DIC concentration, and 0.5 because in carbonate dissolution, only half of the [HCO_3^-] is of atmospheric carbon origin). However, runoff depth ranked almost in reverse order, i.e., from high to low, bare rock, bare soil, crop land, shrub land, grass land. The CSF ranking, from high to low, was grass, crop, shrub, bare rock, bare soil. A new parameter, LCIC (Land use Change Impact on CSF) is defined to compare the impacts of land use change on [DIC] and RD, and evaluate their combined effects on CSF. Compared to bare rock, the absolute values of LCIC (|LCIC|s) were > 1, and CSFs were larger for the three tanks with vegetation cover; CSF is smaller for bare soil, |LCIC| < 1. Finally, it was found that grass land may constitute an optimal land-use for increasing the carbonate weathering-related carbon sink that is critical for carbon management to counter global warming.

1. Introduction

The increase of atmospheric CO_2 is widely considered to be the primary cause of global warming after the Industrial Revolution (Raupach et al., 2007). The imbalance in the calculation of atmospheric CO_2 turnover makes determining precisely where the missing carbon goes a top priority in the study of the carbon cycle (Broecker et al., 1979; Houghton et al., 1999; Joos, 1994; Liu et al., 2010; Melnikov and O'Neill, 2006; Schindler, 1999). The lithosphere, the largest carbon reservoir, should play a central role in the investigation of terrestrial carbon sinks. One major mechanism of atmospheric CO_2 consumption is the reaction with minerals in rocks to form dissolved ions, including bicarbonate (HCO_3^-). The CO_2 reactants are derived either directly from the atmosphere, or indirectly through respiration of plant roots

and microbial activities within soils and pores in rocks, processes which can be viewed as reducing CO_2 emissions to the atmosphere. The HCO_3^- that forms in this reaction is then exported from the terrestrial water system to the oceans where, theoretically, it remains sequestered for millions of years prior to calcite precipitation. Silicate weathering ($CaSiO_3 + CO_2 = CaCO_3 + SiO_2$), rather than carbonate weathering ($CaCO_3 + CO_2 + H_2O \rightleftharpoons Ca^{2+} + 2HCO_3^-$), is regarded as a key mechanism of atmospheric CO_2 consumed by carbonate weathering is thought to be released in the precipitation of calcite (Berner et al., 1983; Curl, 2012; Walker et al., 1981). However, this process occurs on a million-year (geological) time scale. Given that one of the main purposes of modern study of the carbon sink is to control the climate change resulting from human activity, our interest in rock weathering-related carbon sinks is on shorter time scales, i.e., decades to centuries. Moreover, acidification has increased the solubility of $CaCO_3$, in the oceans and thus lengthened the timescale for CO_2 sequestration resulting from carbonate weathering (Feely et al., 2004). The dissolution rate of carbonate is several orders of magnitude faster than that of silicate (Kump et al., 2000; Liu and Dreybrodt, 1997; Plummer et al., 1978). Combined with the biological carbon pump effect (BCP Effect) in which dissolved inorganic carbon (DIC) is transformed into organic carbon (OC) by terrestrial submerged plants and buried (Liu et al., 2015; Liu et al., 2011; Liu et al., 2010; Yang et al., 2016), carbonate weathering-related carbon sinks should be receiving increased attention from researchers.

Carbonate weathering-related carbon sinks vary with climate change (Gislason et al., 2009; Hagedorn and Cartwright, 2008; Tipper et al., 2006; Zeng et al., 2015a) and land use change (Berner, 1992; Raymond et al., 2008; Zeng et al., 2015b; Zhao et al., 2010). Land-use patterns have changed greatly as a result of human activity. Consequently, elucidating the effects of land uses on carbonate weathering will provide scientific evidence for land-use management, as well as making predictions of the potential to increase carbon sinks by changing land uses.

Previous, research into carbonate weathering-related carbon sinks has been conducted at natural sites. However, it is difficult to determine catchment boundaries and runoff due to the complexity of the karst hydrologic systems. Another obstacle is that there is usually a variety of land uses in natural catchments. These issues are challenges for precise investigations of specific land uses on carbonate weathering carbon sinks. As a consequence, the present study was designed and conducted at the Shawan Simulation Test Site, Puding, southwest China.

2. Study site

The simulation test site (Fig. 1, 26°14′–26°15′N, 105°42′–105°43′E, 1200 m asl) is located in Puding County, Guizhou Province, China, which has a humid subtropical monsoon climate. The average annual rainfall is 1225 mm, of which above 80% occurs in the wet season from May to October. The annual mean air temperature is approximately 15.1 °C (Zeng et al., 2015b).

The simulation test site is designed to simulate karst aquifers under different land uses. It consists of five tanks with the identical catchment area (20 m × 5 m), lithology and aquifer properties (porosity = 0.5; aquifer thickness = 2.5 m; Zhu et al., 2015). The tanks are constructed of steel and concrete, coated with epoxy resin to avoid non-karst hydrochemical signals from chemical weathering of the concrete. The aquifers are composed of a limestone-dolomite coarse gravel mix (Guanling Formation, Middle Triassic) from a nearby quarry. The precipitation percolates through pores within coarse gravels. The chemical composition of typical rock and soil at the simulation test site is given in Table 1.

The land-use type for Tank 1 was bare rock consisting only of the carbonate gravel, without soil or vegetation cover, to simulate karst rocky desertification. For Tanks 2, 3, 4 and 5, there was a soil layer (terra rossa taken from nearby) of approximately 50 cm placed over the

gravel. There was no vegetation on the soil in Tank 2, simulating bare land without any agricultural activity. Corn, which is planted in early May and harvested in late August was chosen as a typical crop in Tank 3, simulating cultivated land. The land use in Tank 4 was grass, alfalfa sown in January 2014. Tank 5 had a Roxburgh rose growth, also planted in January 2014, to simulate shrub land (Fig. 1). The land use types in the tanks are physically separated and controlled. As mentioned above, another essential aim of the test site is to simulate the complete drainage of a karst catchment in order to more accurately determine the runoff. Therefore, each tank is discharged by one drain (simulated karst spring, S1 to S5) at the bottom.

3. Methods

3.1. Field monitoring

Field monitoring was conducted from Sept. 1, 2015 to Aug. 31, 2016, covering a complete hydrologic year in order to capture the temporal variations under different land-use treatments. The temporal variations were used to further understand the mechanism of land-use impact on carbonate weathering-related carbon sink by looking at different hydro-chemical response to change in weather conditions under different land-use treatments.

The seasons were defined as autumn (Sept. 1 to Nov. 31, 2015), winter (Dec. 1, 2015 to Feb. 29, 2016), spring (Mar. 1 to May 31, 2016), and summer (June 1 to Aug. 31, 2016). A WTW Technology (Weilheim, Germany) Multiline 350i meter was used to measure water temperature (T), pH and electrical conductivity (EC) with a resolution of 0.1 °C, 0.01 pH unit and 0.1 µS/cm, respectively, at the drain of each tank. The volume concentration of soil CO_2 was measured by a hand-held CO_2 meter (GM 70, Vaisala, Finland) with an accuracy of 10 ppmv. Because there was no soil coverage on the bare rock, Tank 1 CO_2 concentration is equal to the atmospheric CO_2 concentration measured by the GM 70 in the open air, which is also expressed as "soil CO_2" in this study. In each of the four tanks with soil cover, there are six tubes buried to approximately 40 cm depth within the 50 cm soil layer and perforated at the bottom. Soil CO_2 concentration was measured by the probe in each tube. The maximum value measured for each tank was chosen as the soil CO_2 concentration of that tank. Discharges of the five tanks were measured approximately once each month until the rainy season of 2016, when it was increased to three times per month; measurement was by recording the precise time needed to fill a container of 600 ml.

3.2. In situ titration and laboratory analysis

The concentrations of bicarbonate ($[HCO_3^-]$) were measured by in situ titration using an Aquamerck (Damstadt, Germany) alkalinity test kit with an accuracy of 0.05 mmol·L^{-1} (Liu et al., 2007). For other major ions, two sets of 20 ml spring water samples were filtered through 0.45 µm Millipore filters into acid- and purified water-washed high-density polyethylene bottles for conventional anion and cation analysis. Samples for cation analysis were acidified to pH < 2.0 with concentrated nitric acid in order to prevent cation complexing and precipitation. Samples were collected at the time of field monitoring and stored at 4 °C until analyzed at the State Key Laboratory of Environmental Geochemistry, Institute of Geochemistry, Chinese Academy of Sciences. Concentrations of major cations (K^+, Na^+, Ca^{2+}, Mg^{2+}) were determined by inductively coupled plasma optical emission spectrometry (ICP-OES, Varian), and concentrations of major anions (Cl^-, NO_3^-, SO_4^{2-}) by ion chromatography (ICS-90, Dionex; Yang et al., 2015). After grinding rock and soil samples collected at the simulation test site into 75 µm powder and drying at 105 °C, their chemical compositions of rock and soil at the simulation test site were analyzed by using an X-ray fluorescence spectrometer (XRF) in the ALS Laboratory Group. The temperature used for loss on ignition (LOI) was about 1000 °C, at which H_2O and CO_2 were combusted.
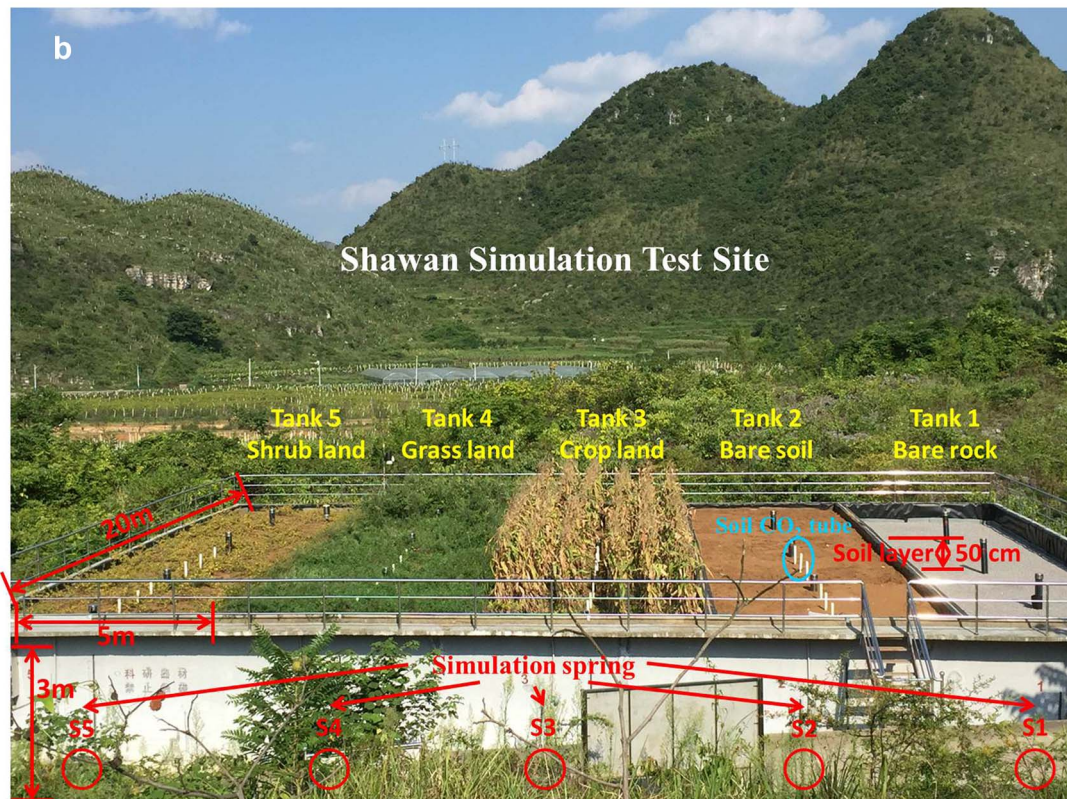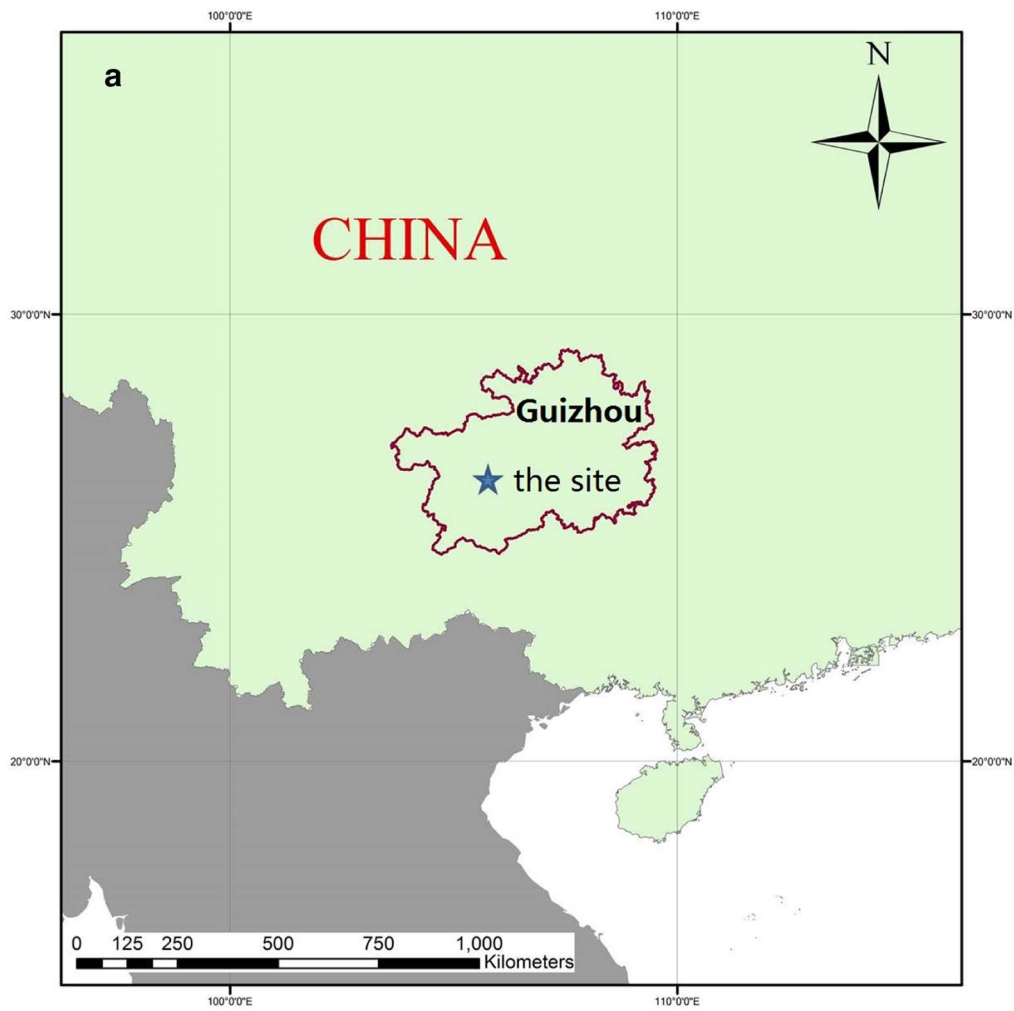
(caption on next page)

Fig. 1. Location (a) and overview (b) of the Shawan Simulation Test Site. White tubes in the tanks are used to measure soil CO_2 concentrations. A drain for the outlet water was installed in the bottom of each tank to simulate the natural underground discharge in a karst system ('karst springs' S1 to S5).

3.3. Estimating CO_2 partial pressure, saturation index, and theoretical equilibrium concentrations of DIC

The CO_2 partial pressure (pCO_2) and saturation index for calcite (SI_C) and dolomite (SI_D) of spring water were calculated by PHREEQC Interactive 3.3.8 (Parkhurst and Appelo, 1999). Measured pH, water temperature, cation, and anion concentrations were used as inputs. The pCO_2, assumed to be in equilibrium with the sampled water, was calculated as:

$$pCO_2 = \frac{(HCO_3^-)(H^+)}{K_H K_1} \tag{1}$$

where the parentheses denote species activity in $mol \cdot L^{-1}$, which are related to concentrations by activity coefficient γ; and K_H and K_1 are the temperature-dependent Henry's Law and first dissociation constants for CO_2 gas in water, respectively. In this study, pCO_2 was calculated to represent the actual concentration of CO_2 in the aquifer for carbonate dissolution. SI_C and SI_D were calculated as:

$$SI_C = log_{10}\left[\frac{(Ca^{2+})(CO_3^{2-})}{K_C}\right] \tag{2}$$

$$SI_D = log_{10}\left[\frac{(Ca^{2+})(Mg^{2+})(CO_3^{2-})^2}{K_D}\right] \tag{3}$$

where K_C and K_D are the temperature-dependent equilibrium constants for calcite and dolomite, respectively (Drever, 1988; Stumm and Morgan, 1981). Where $SI > 0$, the water is oversaturated with respect to the mineral; if $SI < 0$, the water still has corrosion capacity with respect to the mineral; at $SI = 0$, equilibrium is reached.

Theoretical equilibrium concentrations of DIC from the dissolution of calcite ($[DIC]_C$) and dolomite ($[DIC]_D$), which are the two chief types of carbonate minerals, were calculated at a given pCO_2 gradient with the software EQILCAMG (Dreybrodt, 1988). They were calculated to make a comparison with the measured [DIC] and to further understand the mechanism of land-use impact on [DIC] by looking at the relationship between equilibrium [DIC] and pCO_2.

3.4. Calculation of annual evapotranspiration, infiltration coefficients, and runoff depth

The evapotranspiration (ET) and infiltration coefficient (α) are important parameters to evaluate the strength of hydrologic cycles. Evapotranspiration was calculated as follows:

$$ET = P - Q/A - \Delta H \times \mu \tag{4}$$

$$ET = P - Q/A - (H_T - H_I) \times \mu \tag{5}$$

$$ET = P - RD - (H_T - H_I) \times \mu \tag{6}$$

where P denotes the annual precipitation in $m \cdot a^{-1}$; Q denotes spring discharge in $m^3 \cdot a^{-1}$; A denotes catchment area in m^2; RD (Q/A) denotes runoff depth in $m \cdot a^{-1}$ with "a" referring to "annum or year"; ΔH is the difference of terminal water level (H_T) and initial water level (H_I)

of a hydrologic year in $m \cdot a^{-1}$; μ is the porosity of the aquifer (0.5 in this study); and the unit of ET is $m \cdot a^{-1}$.

The infiltration coefficient (α) was calculated as follows:

$$\alpha = (P - ET)/P \tag{7}$$

$$\alpha = \{P - [P - RD - (H_T - H_I) \times \mu]\}/P \tag{8}$$

$$\alpha = [RD + (H_T - H_I) \times \mu]/P \tag{9}$$

3.5. Calculation of the carbonate weathering-related carbon sink flux

The carbonate weathering carbon sink flux (CSF) was calculated as follows (Liu et al., 2010):

$$CSF = 0.5 \times 12 \times Q \times [DIC]/A \tag{10}$$

$$CSF = 6 \times RD \times [DIC] \tag{11}$$

where CSF is in $t \cdot C \cdot a^{-1} \cdot km^{-2}$ with "C" representing carbon; the factor 0.5 results from the fact that, in the case of carbonate dissolution, only half of the $[HCO_3^-]$ is of atmospheric origin; 12 denotes the molecular weight of carbon; and DIC consists of carbonic acid, bicarbonate, and carbonate ions. The proportion of these DIC components depends on the pH value. If pH ranges from 7 to 9, 95% of the DIC exists as bicarbonate ions. In most cases of karst waters, the species of H_2CO_3 and CO_3^{2-} can be neglected. Thus, in this study, [DIC] is close to the concentration of bicarbonate ($[HCO_3^-]$) in $mmol \cdot L^{-1}$.

The CSF should have contained uncertainty due to the RD measurement and mean [DIC] calculation. According to error propagation theory, the potential root mean square error of CSF can be estimated by:

$$\left(\frac{\sigma_{CSF}}{CSF}\right)^2 = \left(\frac{\sigma_{RD}}{RD}\right)^2 + \left(\frac{\sigma_{[DIC]}}{[DIC]}\right)^2 \tag{12}$$

where σ is the standard deviation.

4. Results

The hydrochemical facies of the five simulated spring waters under different land uses are shown in a Piper diagram in Fig. 2. The major cations are Ca^{2+} and Mg^{2+}, and the major anion is HCO_3^-. The hydrochemical type is a simple HCO_3-Ca-Mg, which is typical karst water. Cation concentrations in spring water samples from the five tanks were quite similar. The proportions of HCO_3^- in anions showed remarkable differences with the different land uses. The proportion of HCO_3^- in the grass land was the largest and clearly differed from the others; seasonal variations of hydrochemical composition for the tanks were also minor except in the grass land, which will be discussed below.

4.1. Temporal variations of hydrological parameters under different land uses

4.1.1. Evapotranspiration (ET) and infiltration coefficient (α)

The complete hydrological year from Sept. 1, 2015 to Aug. 31, 2016

Table 1
Chemical compositions of rock and soil samples from the Shawan Simulation Test Site, Southwest China.

Chemical composition	Al_2O_3	BaO	CaO	Cr_2O_3	Fe_2O_3	K_2O	MgO	MnO	Na_2O	P_2O_5	SiO_2	SrO	TiO_2	LOI[a]	Total
	(%)														
Rock sample	0.51	0.02	46.15	< 0.01	0.31	0.22	7.40	< 0.01	0.03	0.01	1.42	0.08	0.04	44.03	100.19
Soil sample	22.04	0.02	0.64	0.02	9.70	0.85	1.60	0.32	0.10	0.24	49.31	0.01	1.48	12.68	99.01

[a] LOI is an abbreviation for Loss On Ignition at about the temperature of 1000 °C.

Legend

- 🟦 Bare rock
- ⚫ Bare soil
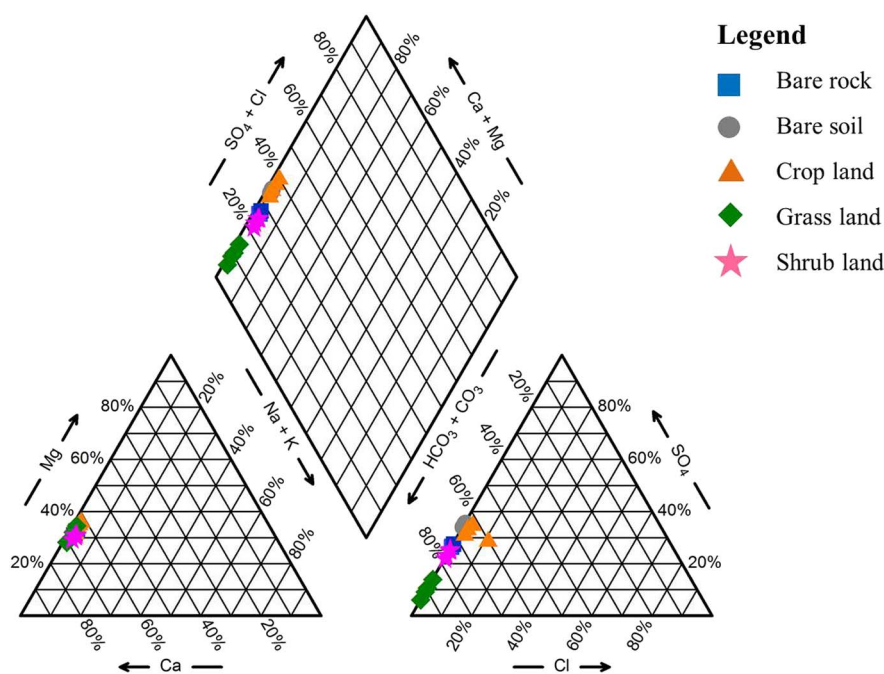- 🔺 Crop land
- 🟢 Grass land
- ⭐ Shrub land

Fig. 2. Hydrochemical facies of the simulated springs under the five different land uses. Four data points for each land use represent the four seasonal average hydrochemical compositions. The hydrochemical type can be described as HCO_3-Ca-Mg, typical karst water.

Table 2
Hydrologc and carbon sink fluxes (CSF) under different land-uses[a].

Site	Annual rainfall (mm·a^{-1})	Annual discharge (m^3·a^{-1})	Water level change (m)	Annual evapotranspiration[b] (mm·a^{-1})	Infiltration coefficient[c]	RD[d] (m·a^{-1})	[DIC][e] (mean ± STD) (mmol·L^{-1})	CSF[f] (mean ± STD) (t·C·a^{-1}·km^{-2})
Bare rock	1375.4	116.408	0.197	112.8	0.92	1.16	1.68 ± 0.17	11.70 ± 1.22
Bare soil		89.276	− 0.222	593.6	0.57	0.89	1.72 ± 0.21	9.23 ± 1.11
Crop land		86.622	− 0.236	627.2	0.54	0.87	2.57 ± 0.33	13.36 ± 1.73
Grass land		60.769	− 0.254	894.7	0.35	0.61	4.56 ± 0.67	16.63 ± 2.43
Shrub land		75.994	− 0.275	753.0	0.45	0.76	2.74 ± 0.34	12.47 ± 1.57

[a] The time period in this table is from Sept.1, 2015 to Aug. 31, 2016, a complete hydrologic year.

[b] The annual evapotranspiration is calculated as follows: evapotranspiration = rainfall-discharge / area-water level change.

[c] The infiltration coefficient is calculated as follows: infiltration coefficient = (rainfall-evapotranspiration) / rainfall.

[d] RD (runoff depth) is calculated as follows: RD = discharge / area.

[e] The mean [DIC] is calculated according to the discharge weight.

[f] The CSF is calculated as follows: CSF = 6 × RD × [DIC].

was chosen as a unit for the investigation of ET and α. Since over 90% of the rainfall directly recharged the bare rock aquifer, the amount of evaporation from it was the least among the five tanks. Almost 70% of rainfall was evapotranspired on the grass land, the largest of the five tanks. This made the α of grass land the smallest. The amount of evapotranspiration for shrub land was also large, over 50% of rainfall; α was the second smallest. The amounts of evapotranspiration for bare soil and crop land were almost the same, and so were α (Table 2).

4.1.2. Runoff depth (RD)

The only recharge source for the simulated aquifers in this study was rainfall, and thus RD varied with it, but with a three-month time lag behind rainfall (Fig. 3). Seasonal rainfall ranking, high to low, was summer, autumn, spring, and winter. The RD of tanks, except for shrub land, ranked from high to low, was autumn, winter, summer and spring, exactly a one-season lag behind the rainfall. Although the runoff depths of spring and winter switched their ranking for the shrub land, the difference between them was slight (< 1 m^3·season^{-1}). Like ET and α, RD also showed some remarkable differences between land uses. Bare rock drained the largest amount of water, almost twice that of grass land, the least. RD decreased sequentially through the bare soil, crop and shrub tanks.

4.2. Temporal variations in soil CO_2 and DIC concentrations under the different land uses

4.2.1. Soil CO_2 concentration and partial pressure of CO_2 (pCO_2) in water

Except for the case bare rock, the measured soil CO_2 concentrations exhibited similar seasonal variation patterns, i.e., higher in summer and autumn and lower in winter and spring. CO_2 concentration in the bare rock tank was more stable, without remarkable seasonal variation (Fig. 4c). The annual mean soil CO_2 concentration of the grass land ranked first, > 18 times higher than the last, i.e., bare rock. The shrub and crop lands were second and third but with only small differences. The annual mean soil CO_2 concentration in the bare soil was an order of magnitude lower than in the tanks with vegetation cover, just slightly higher than the bare rock (Table 3). The temporal patterns of variation of pCO_2 in the water were almost the same as soil CO_2 concentrations. Because of the diffusion of soil CO_2 into the atmosphere, soil CO_2 concentrations measured in situ were lower than the pCO_2 calculated by PHREEQC, which could reflect the actual concentration of CO_2 in the aquifer that was available for carbonate dissolution (Fig. 4c).

4.2.2. Concentration of DIC ([DIC])

Temporal variations of [DIC] for S1 to S5 can be divided into two types. In the tanks with vegetation cover, [DIC] exhibited remarkable
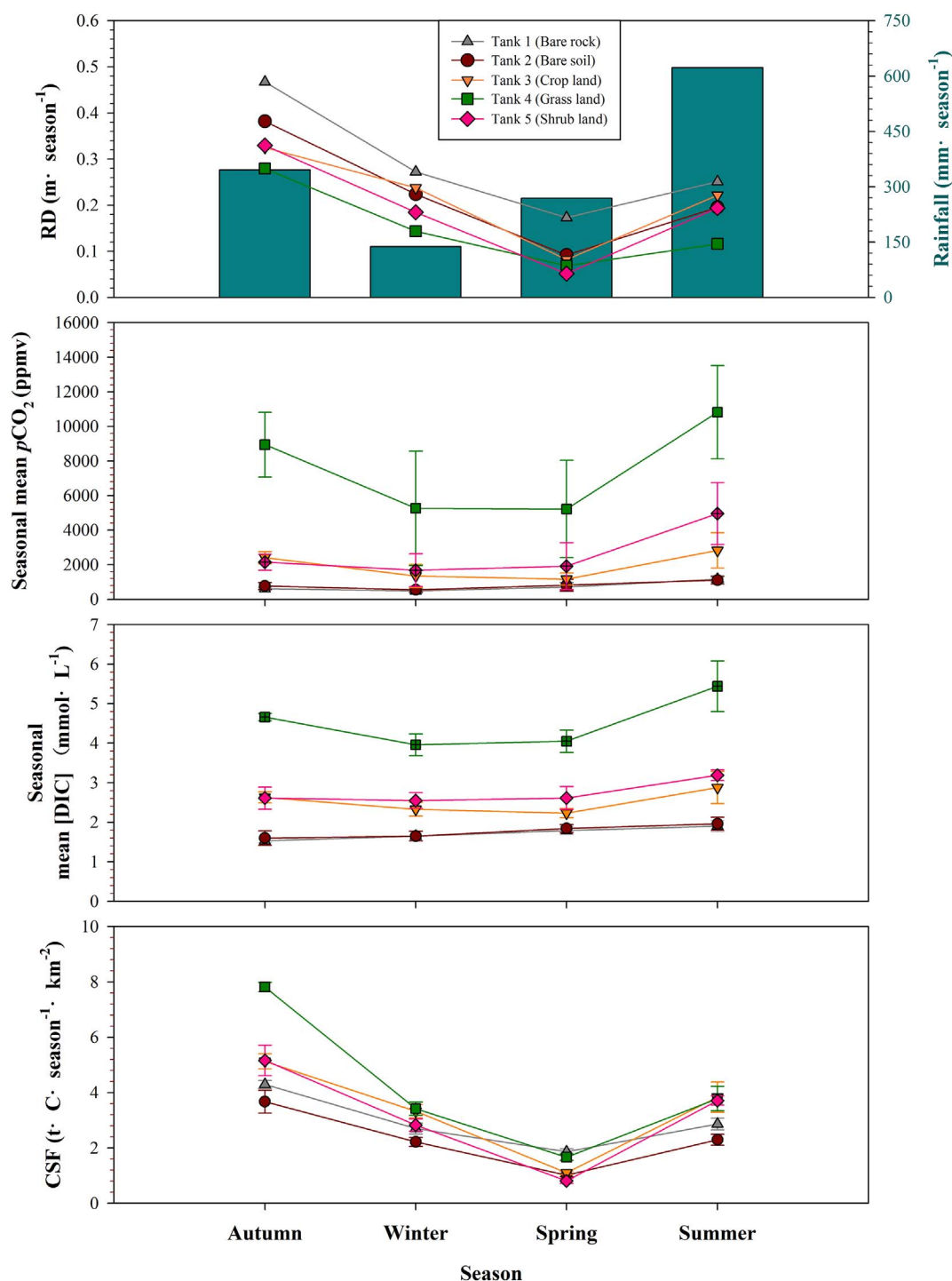
Fig. 3. Time series of pCO$_2$, [DIC], runoff depth (RD), and CSF for the five land uses. Standard deviation error bars for pCO$_2$, [DIC] and CSF are shown. The RD are measured data, any systematic error is smaller than the symbol.

seasonal variation, higher in summer and autumn and lower in winter and spring. The tanks without vegetation showed less seasonal variation (Figs. 3 and 4c). There were some notable differences. Grass land had the highest annual mean [DIC], 4.56 ± 0.67 mmol·L^{-1}, almost three times that of the lowest, 1.68 ± 0.17 mmol·L^{-1} on the bare rock. Shrubs, crops, and bare soil ranked second, third and fourth respectively (Tables 2 and 3, Fig. 5).

4.3. Temporal variations of CSF under different land uses

The same patterns of seasonal variation in CSF were measured in all

five tanks: the largest CSF occurred in autumn, followed by summer, winter, and spring (Fig. 3). The annual CSF varied between tanks, grass land having the largest value (~17 t·C·a^{-1}·km^{-2}), followed by crop land (~13 t·C·a^{-1}·km^{-2}), shrub land (~12 t·C·a^{-1}·km^{-2}), bare rock (~12 t·C·a^{-1}·km^{-2}), and bare soil (~9 t·C·a^{-1}·km^{-2}).

5. Discussion

As shown in Eq. 11, CSF is the product of [DIC] and RD. Land use change affects CSF through its impacts on both [DIC] and RD.
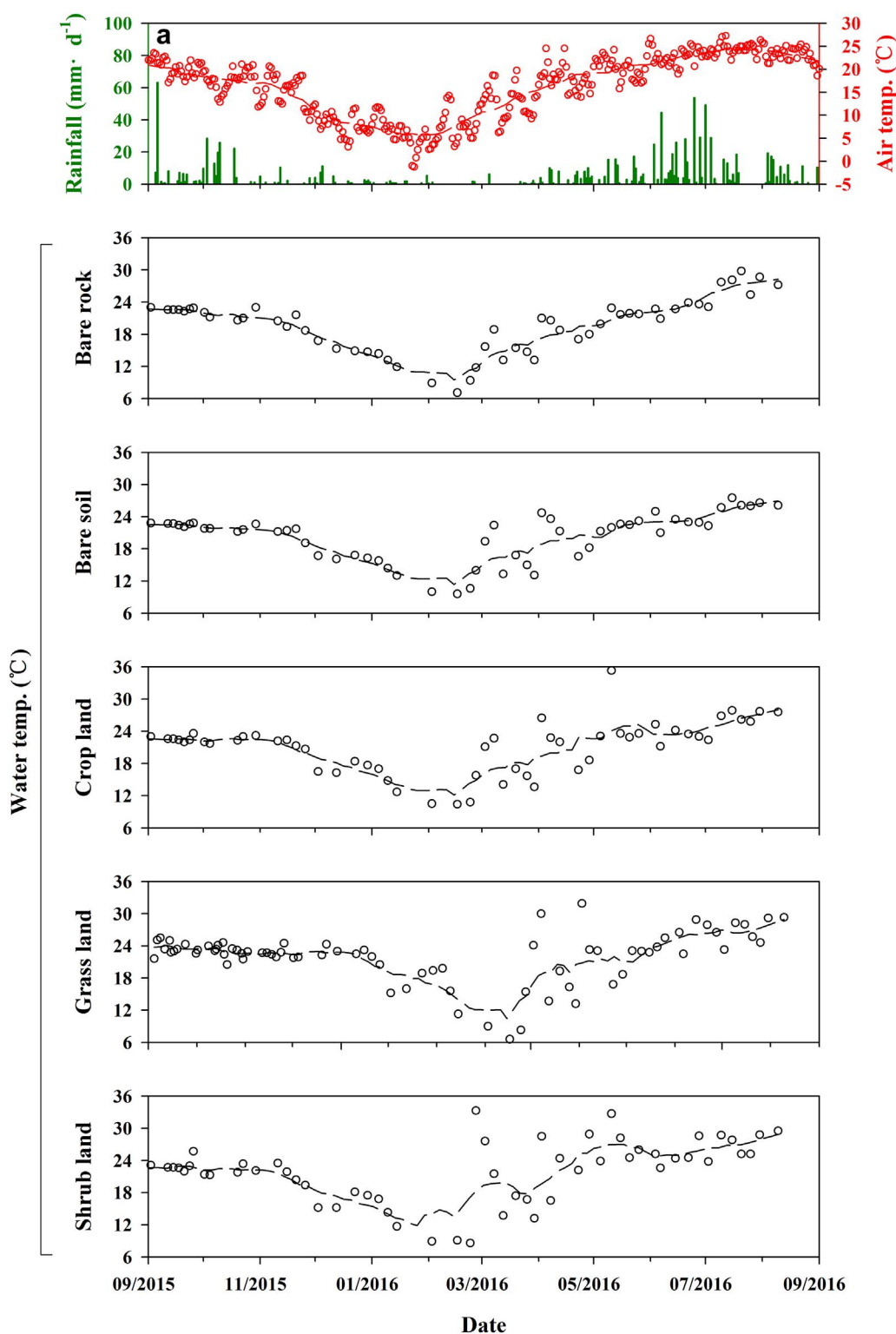
Fig. 4. Time series for soil CO_2 and hydrochemical parameters. (a) to (d) represent water temperature, pH, soil CO_2 (pCO_2)-[DIC], and SI_C-SI_D, respectively. Dashed lines represent data curves smoothed by using a linear polynomial regression and weights computed from the Gaussian density function. The meteorological data was obtained from the meteorological station of Puding Karst Ecosystem Research Station, Chinese Academy of Sciences.

5.1. Impact of land use change on [DIC]

In this study, spring waters were generally slightly saturated with respect to calcite (Fig. 4d). The similarities of temporal variations between [DIC] and pCO_2 indicated that the equilibrium [DIC] is determined by carbonate weathering, which is driven by pCO_2, the latter varying with land use. Fig. 6 shows the equilibrium [DIC] as a function of pCO_2 for chemical weathering of calcite and dolomite, respectively, at the local annual mean temperature of 15.1 °C. Because the lithology

is a combination of limestone and dolomite, the five types of land use [DIC] measured, in general, fell in the ranges of equilibrium [DIC] for chemical weathering of calcite and dolomite at a given pCO_2 gradient (Fig. 6). In addition, they exhibited a synchronous increasing trend with pCO_2, which has also been found in some other field studies (Andrews and Schlesinger, 2001; Liu and Zhao, 2000; Zhao et al., 2010).

The [DIC] synchronously increasing trend with pCO_2 suggests that temporal variations of [DIC], one of the two factors in the CSF calculation, can be explained by the changes in soil CO_2 concentration (Liu
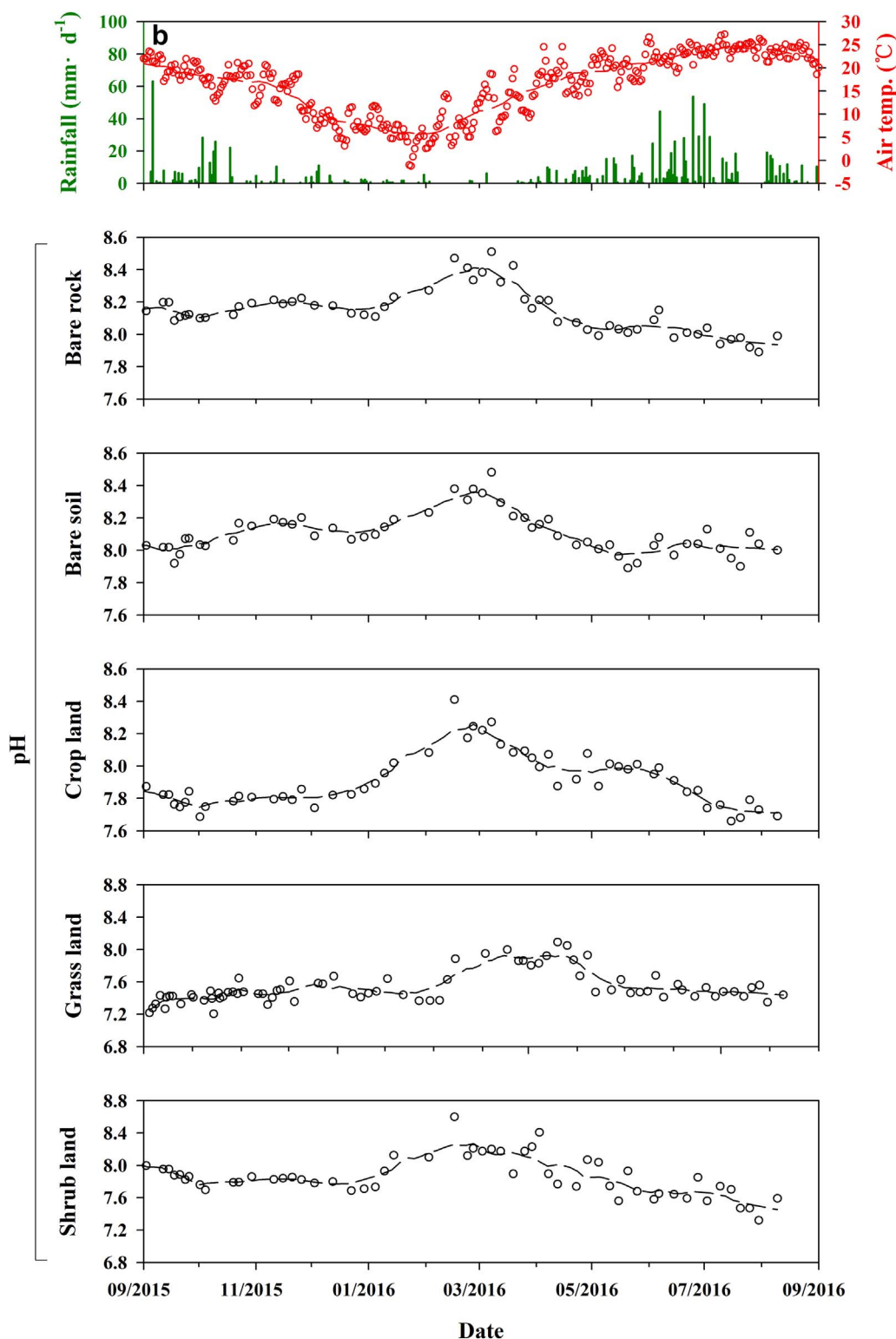
Fig. 4. (continued)

and Zhao, 2000), due chiefly to root respiration and microbial activity. The growth of vegetation benefits from the warmer climate in summer and autumn and more abundant rainfall than in winter and spring. Root respiration is enhanced, leading to increase of soil CO_2 production. Meanwhile, more CO_2 would be released by the decomposition of soil organic matter from microbial activities in the soil and rock pores. Consequently, [DIC] from the tanks with soil, especially those with vegetation cover, showed significant seasonal variation patterns (Figs. 3 and 4c). Differences of pCO_2 among the five tanks were a reflection of

the different land use change. Fig. 6 shows the positive correlation between pCO_2 and [DIC]. The higher soil CO_2 of the grass land led to higher annual mean [DIC]. Compared to the vegetated tanks, bare soil was lacking in CO_2, and thus its annual mean [DIC] was lower. Similarly, the bare rock had the lowest annual mean [DIC] (Fig. 5).

5.2. Impact of land use change on RD

As shown in Fig. 5, the RD of land use with high [DIC] was low.
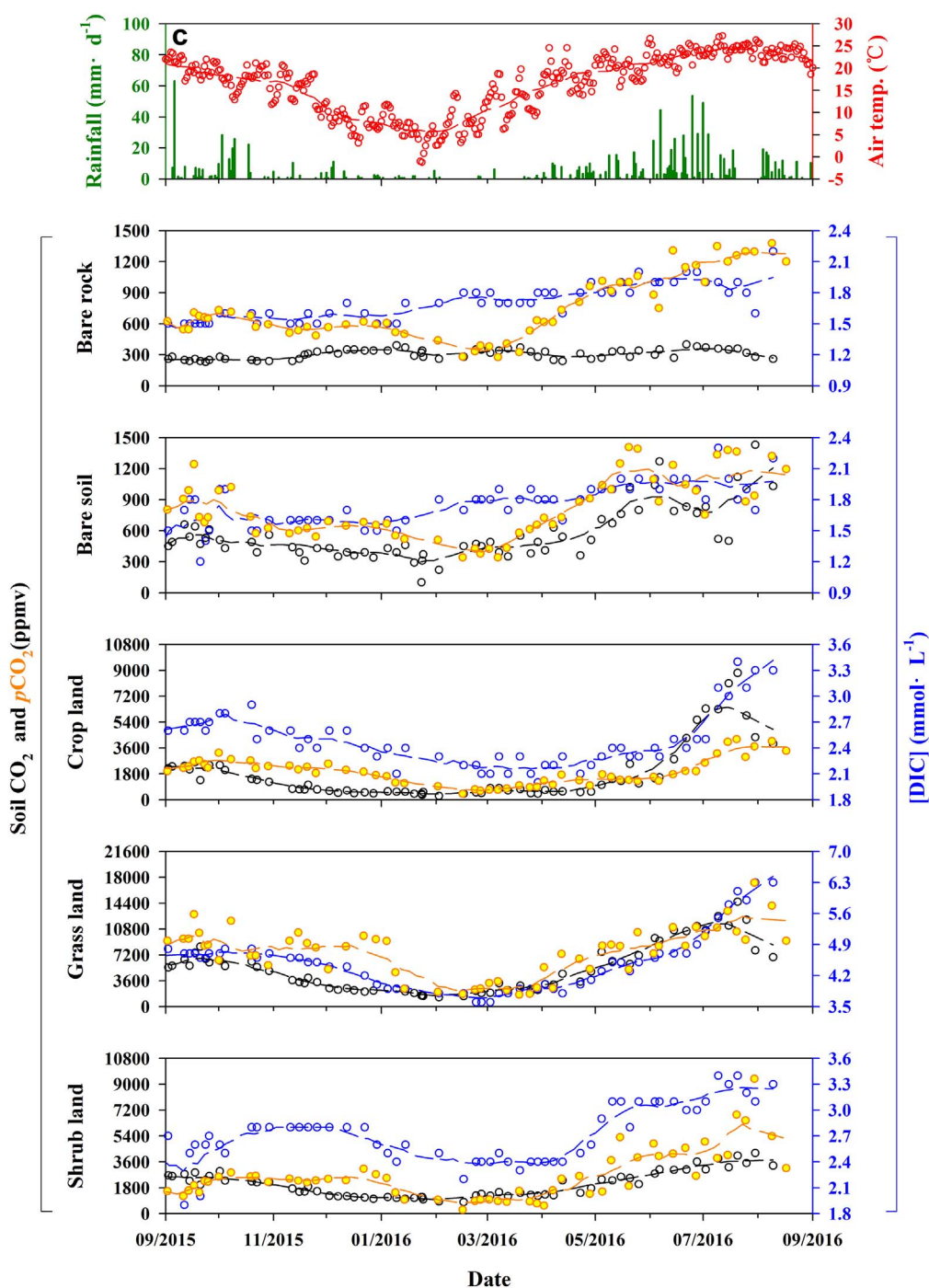
Fig. 4. (continued)

Fig. 5 indicates that land use changes can have opposite impacts on runoff and DIC production. For the five tanks, since rainfall was the same, differences in RD were due to the varied evapotranspiration caused by the five different land uses. Grass land had the greatest biomass, and thus the highest evapotranspiration and the lowest runoff. On the shrub land, Roxburgh rose leaves were sparse, and had not developed maturely; thus, evapotranspiration was less than on the grass, resulting in a relatively higher RD. On the crop land, the growth period of corn (May to August) was only one third of the year, with the result that it did not differ greatly from the bare soil results; evapotranspiration was lower than on the shrubs and grass. With neither soil nor vegetation, evapotranspiration on the bare rock with zero transpiration was the lowest and the runoff was the highest.

5.3. Impact of land use change on CSF

As discussed above, CSF is a product of two factors, [DIC] and RD, which were impacted in opposite directions by the different land uses. This substantially complicates the accurate evaluation of the impact of land use change on CSF. Therefore, it is essential to compare impacts on [DIC] and RD accurately, and establish the mathematical relations among variations of [DIC], RD, and CSF. Zeng et al. (2015b) chose the absolute differences (Δ[DIC] and ΔRD) to evaluate the impacts. How-ever, this method may be inadequate to evaluate impacts on CSF based on the impacts on [DIC] and RD, because the calculation of CSF is a multiplication rather than an addition. In addition, previous research has usually been conducted in field sites with numerous non-controlled variables, implying that the type of land use is not the sole factor that
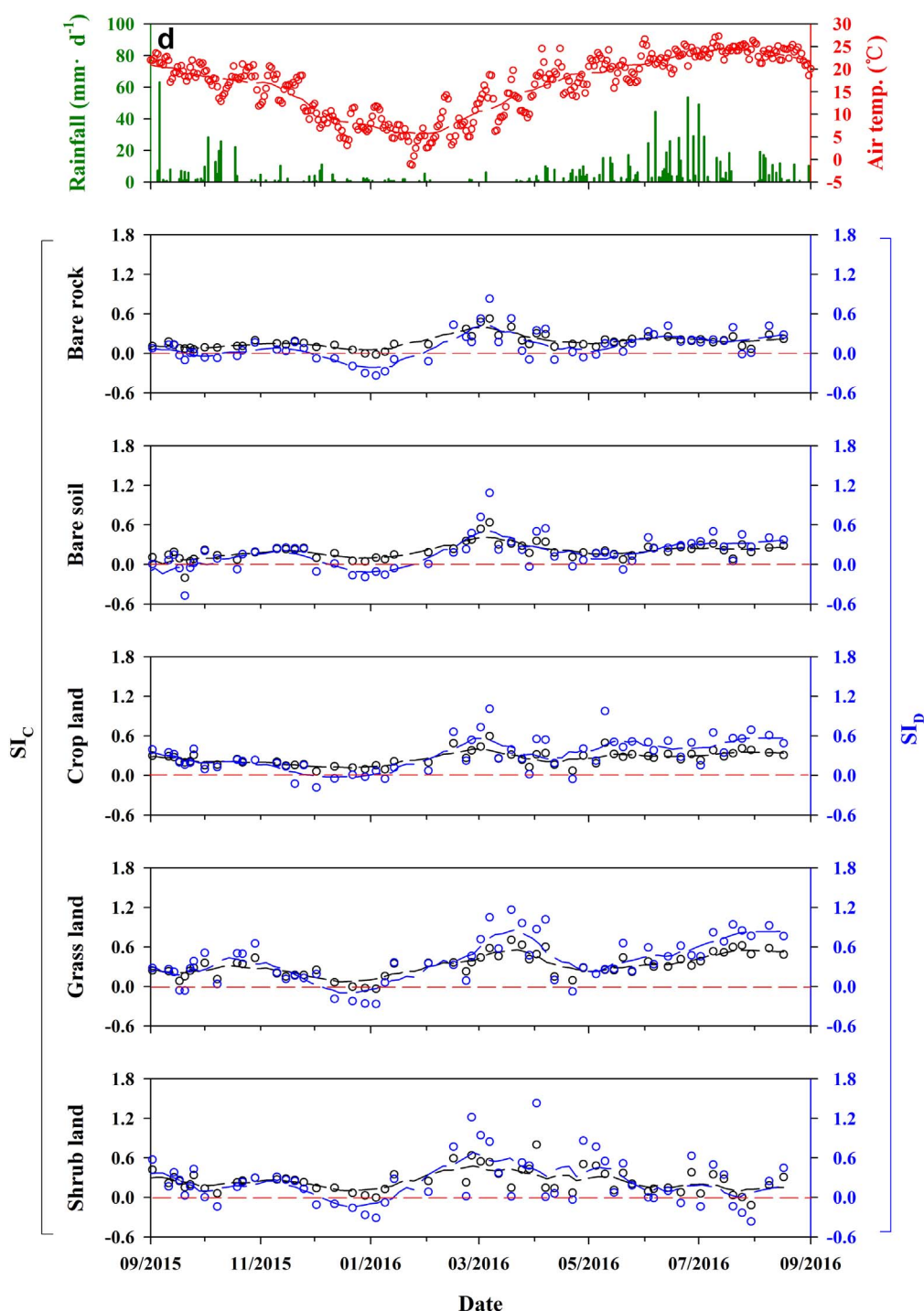
Fig. 4. (continued)

could have an influence on [DIC], RD, and CSF. Accordingly, a parameter which can compare impacts of land use change on [DIC] and RD, and can then be utilized to evaluate the impact on CSF, is defined in this study for the first time. Termed LCIC (Land use Change Impact on CSF), $LCIC_N$ is calculated as follows:

$$LCIC_N = \frac{\left(\frac{[DIC]_N - [DIC]_1}{[DIC]_1}\right) \times 100\%}{\left(\frac{RD_N - RD_1}{RD_1}\right) \times 100\%} \quad (N = 2, 3, 4, 5) \tag{13}$$

where the subscript number denotes the tank number in this study.

As noted, the calculation of CSF was a multiplication, combined

with the ranges of fluctuation of [DIC] and RD, which were different by orders of magnitude. Therefore, changes of absolute values of [DIC] and RD might not be appropriate to evaluate the trends in the CSF results. Consequently, the new parameter, LCIC, was defined by comparing the variability of [DIC] and RD impacted by land use change. The terms $([DIC]_N - [DIC]_1) / DIC_1$ and $(RD_N - RD_1) / RD_1$ denote the variability of [DIC] and RD, respectively.

In this study, the bare rock (Tank 1) was chosen as a reference standard because it is representative of an extreme environment without soil and vegetation. The effects of soil and vegetation on CSF can be determined by comparison with it. Normally, LCIC was expected to be negative due to the competitive relationship between [DIC]

Table 3
Statistics of physiochemical parameters of water from simulated springs and soil CO_2 concentrations under different land uses[a].

Site	Bare rock				Bare soil				Crop land				Grass land				Shrub land			
	Min.	Max.	Mean	c.v.[b]	Min.	Max.	Mean	c.v.	Min.	Max.	Mean	c.v.	Min.	Max.	Mean	c.v.	Min.	Max.	Mean	c.v.
Water temp.(°C)	7.1	29.8	19.8	25.7	9.6	27.5	20.1	22.2	10.4	27.9	20.6	22.0	6.6	29.3	20.8	26.0	8.6	29.5	20.6	26.1
pH	7.89	8.51	8.14	1.7	7.89	8.48	8.10	1.5	7.66	8.41	7.91	2.1	7.32	8.09	7.58	2.7	7.32	8.60	7.86	3.1
[DIC] (mmol/L)	1.50	2.20	1.68	10.4	1.20	2.30	1.72	12.1	2.00	3.40	2.57	13.0	3.60	6.30	4.56	14.6	1.90	3.40	2.74	12.6
SI_C	−0.02	0.53	0.18	55.9	−0.20	0.64	0.20	31.3	0.06	0.60	0.26	54.9	−0.04	0.71	0.32	49.1	−0.12	0.80	0.25	48.1
SI_D	−0.34	0.83	0.11	49.1	−0.47	1.08	0.17	38.7	−0.18	1.01	0.32	52.0	−0.27	1.16	0.4	52.5	−0.37	1.43	0.25	60.9
Soil CO_2 (ppmv)	230	400	306	15.2	100	1430	562	45.3	260	8820	1769	110.0	1290	14,590	5186	63.7	790	4210	2021	44.0
pCO_2 (ppmv)	276.00	1377.50	746.00	40.9	340.8	1406.7	819.9	36.3	408.4	4200.5	1945.1	47.9	1673.8	17,258.4	7592.6	46.4	258.3	9377.8	2642.5	66.6

Because the values of SI_C and SI_D could be positive or negative, c.v. for SI values were determined after the SI values were normalized to zero.

[a] The sampling period was from Sept. 1, 2015 to Aug. 31, 2016.

[b] Coefficient of variation (c.v.) = (standard deviation / average value) × 100%.

increase and RD decrease induced by the differing land uses. Therefore, the absolute value of LCIC (|LCIC|) was utilized to compare the impact of land use differences on [DIC] and RD. |LCIC| < 1 denotes that land use difference-induced RD decrease had a greater impact than [DIC] increase; |LCIC| > 1 denotes that difference-induced [DIC] increase had a greater impact than RD decrease. The absolute difference of CSF (ΔCSF) was chosen to test and verify the reliability of |LCIC|:

$$\Delta CSF_N = CSF_N - CSF_1 (N = 2, 3, 4, 5) \tag{14}$$

ΔCSF$_N$ calculated for the whole hydrologic year and four seasons separately are plotted versus the corresponding |LCIC$_N$| in Fig. 7 and presented in Table 4.

Fig. 7 could be divided into four zones. The upper zones with ΔCSF > 0 represented CSF increase, while lower zones with ΔCSF < 0 represented CSF decrease. The lefthand zones with |LCIC| < 1 represented the cases where land use difference-induced RD decrease predominated over [DIC] increase, and the righthand zones with |LCIC| > 1 where [DIC] increase was predominant. In Fig. 7 the data fall chiefly in two zones an upper-right zone of [DIC] increase-induced CSF increase and a lower-left zone of RD decrease-induced CSF decrease. Data plotting in the RD decrease-induced CSF decrease zone are either those of the spring season (green points) or of bare soil (circles). In the first case, low temperatures during the spring months restricted root respiration and organic decomposition, leading to lower [DIC] and limited land use difference-induced [DIC] increases. The decreased RD was clearly due to the minimal rainfall. The reason that this occurred in the spring season rather than the winter was the one-season time lag of RD behind precipitation, as described above. In this situation, the variability of RD was higher than that of [DIC] in the spring, and CSF of the tanks with soil and/or vegetation cover was lower than the CSF of the bare rock. In the second case, compared to bare rock, the bare soil (Tank 2) contributed little to the [DIC] increase, but greatly to the RD decrease, which resulted in a decrease of CSF, regardless of the season. These two cases could be classified into RD decrease-induced CSF decreasing caused by land use difference with |LCIC| < 1 and ΔCSF < 0. All other data points plotted in the [DIC] increase-induced CSF increase zone because the change from bare rock to vegetation cover had a greater impact on increasing [DIC] than reducing RD in all seasons except spring. In other words, in this situation, the influences of the RD decrease resulting from increasing evapotranspiration could not counteract the influences of the [DIC] increase from increasing vegetation cover. This indicates that root respiration played a dominant role in increasing CSF. As an outlier, the grass land in springtime (Point A in Fig. 7) was with |LCIC| > 1 and ΔCSF < 0; although the CSF for the grass was less than that for bare rock in spring, the difference between them was slight (ΔCSF close to 0) due to the higher rate of increase of [DIC] compared to the rate of decrease of RD (|LCIC| > 1).

There was a statistically significant positive correlation between ΔCSF and |LCIC|. The larger the difference between the rate of increase of [DIC] and rate of decrease of RD, the greater the contribution to the carbonate weathering-related carbon sink. Only one data point deviated far from the regression line, i.e., for grass land in autumn (Point B in Fig. 7). Autumn was a season favoring rapid [DIC] growth in the grass due to abundant rainfall and high temperatures. Consequently, CSF for grass increased sharply in autumn, creating the large deviation.

Fig. 7 suggests that, even though increase of [DIC] will be accompanied by decreasing RD from the bare rock to soil and/or vegetation cover, as long as the amplification of [DIC] was larger than the reduced amplitude of RD (|LCIC| > 1), the formation of the carbonate weathering-related carbon sink will be promoted. In addition, the larger the difference in amplitude, the more the CSF. This demonstrated the dominant role of soil CO_2 production in controlling CSF across the different land uses. As noted, for a given land use, CSF exhibited a similar pattern of temporal variation, with RD playing the dominant role in controlling CSF, which confirms a previous study in this geographical region (Zeng et al., 2015b). In the present study, we focused on the
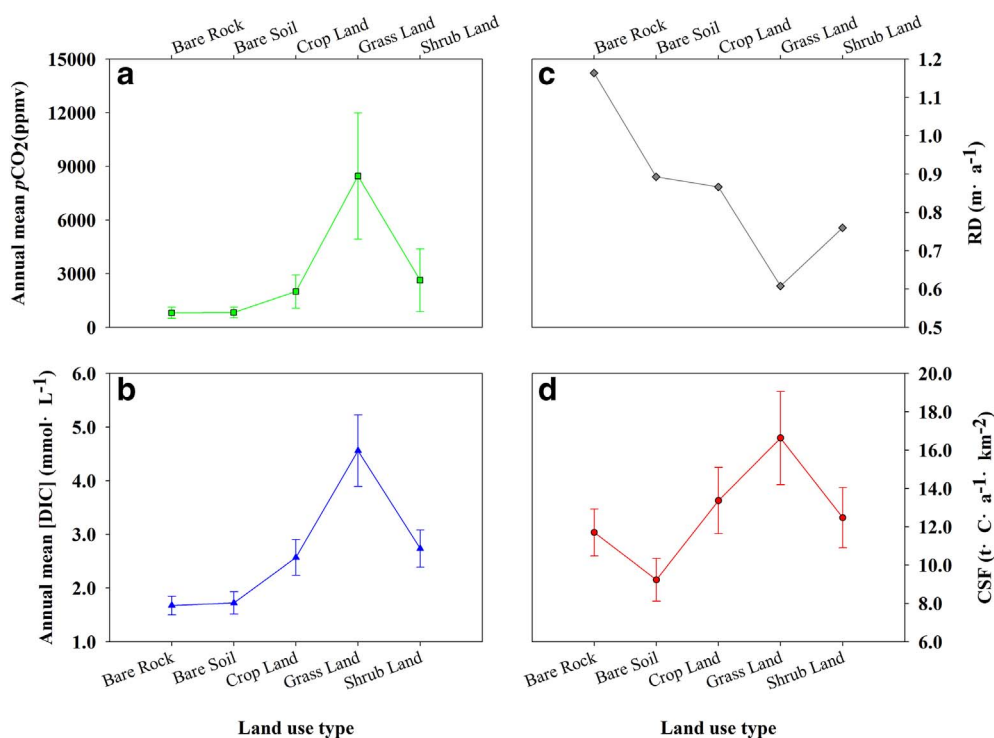
Fig. 5. Annual mean pCO_2, [DIC], RD, and CSF under different land-use treatments. Standard deviation error bars for pCO_2, [DIC] and CSF are shown. The RD are measured data, any systematic error is smaller than the symbol.
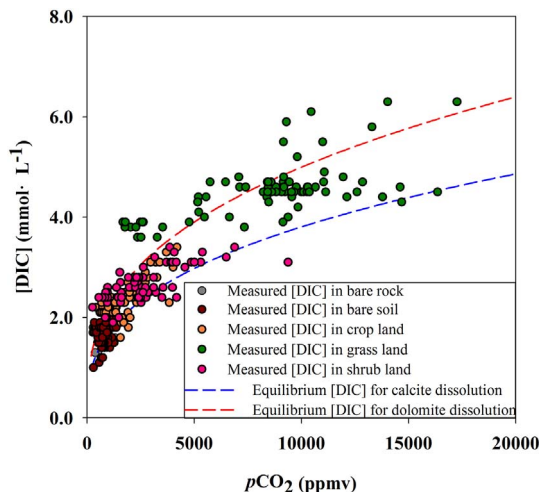

Fig. 6. The relationship between equilibrium [DIC] and pCO_2. Equilibrium DIC concentrations were calculated at 15.1 °C, the local annual mean temperature.

impacts of different land uses on CSF. It was found that the grass land had a significant advantage in carbon sequestration, and that vegetation cover facilitated soil CO_2 production, and thus CSF.

6. Conclusions

This study, for the first time, applies rigorous control of the variables encountered in research on the impacts of different land uses on carbonate weathering carbon sinks by undertaking the investigations in a simulation test field. This avoids potential errors in measuring catchment boundaries and runoff in natural karst basins. The results show that different land uses affects CSF by controlling [DIC] and RD via differing soil CO_2 production and evapotranspiration respectively. Normally, changing land use from bare rock to any other will decrease RD, while increase [DIC]. Change of CSF is the combined result of the changes of RD and [DIC]. A novel parameter, LCIC, is defined here for the first time in order to compare the

effects of different land uses change on [DIC] and RD, and evaluate their combined effect on CSF. |LCIC| > 1 indicates that CSF will increase because land use-induced increase of DIC predominates. |LCIC| < 1 indicates that CSF will decrease because land use-induced decrease of RD exceeds the effects of the DIC increase. In the study year, it was found that the bare soil experiment with |LCIC| < 1 was unfavorable for carbonate weathering-related carbon sequestration ($9.23 \pm 1.11 \, t \cdot C \cdot a^{-1} \cdot km^{-2}$, even lower than the bare rock experiment). However, compared to bare rock ($11.70 \pm 1.22 \, t \cdot C \cdot a^{-1} \cdot km^{-2}$) the experiments with vegetation cover were beneficial, significantly increasing the carbon sink, with shrub land ($12.47 \pm 1.57 \, t \cdot C \cdot a^{-1} \cdot km^{-2}$), crop land ($13.36 \pm 1.73 \, t \cdot C \cdot a^{-1} \cdot km^{-2}$), and grass land ($16.63 \pm 2.43 \, t \cdot C \cdot a^{-1} \cdot km^{-2}$). For these three types of land uses, |LCIC| are all > 1.
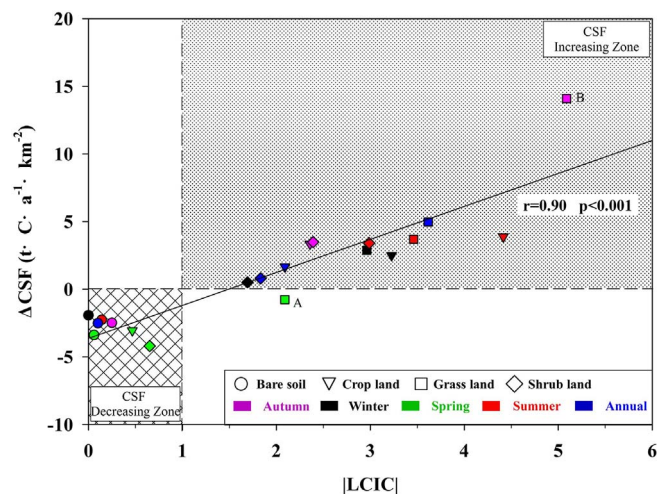

Fig. 7. The relationship between ΔCSF and a newly defined parameter |LCIC|. The dotted area indicates the CSF increasing zone determined by land-use change-induced DIC increase, while the gridded area indicates the CSF decreasing zone determined by land-use change-induced runoff decrease. The regression line represents the linear relationship between ΔCSF and |LCIC|. The p-value was calculated by using SPSS Statistics. A, B: two outlying data points -see the text for details.

Table 4
Results for LCIC and ΔCSF[a].

Season	Parameter	Bare soil	Crop land	Grass land	Shrub land
Autumn	ΔRD[b]	− 0.341	− 0.570	− 0.752	− 0.552
	ΔC[c]	0.07	1.10	3.13	1.08
	%ΔRD[d]	− 18.26%	− 30.49%	− 40.20%	− 29.51%
	%ΔC[e]	4.58%	71.90%	204.58%	70.59%
	ΔCSF[f]	− 2.49	3.34	14.10	3.48
	LCIC[g]	− 0.25	− 2.36	− 5.09	− 2.39
	|LCIC|[h]	0.25	2.36	5.09	2.39
Winter	ΔRD	− 0.195	− 0.139	− 0.515	− 0.351
	ΔC	0.00	0.68	2.31	0.90
	%ΔRD	− 17.93%	− 12.77%	− 47.24%	− 32.21%
	%ΔC	0.00%	41.21%	140.00%	54.55%
	ΔCSF	− 1.93	2.50	2.87	0.51
	LCIC	0.00	− 3.23	− 2.96	− 1.69
	|LCIC|	0.00	3.23	2.96	1.69
Spring	ΔRD	− 0.325	− 0.365	− 0.418	− 0.486
	ΔC	0.05	0.44	2.26	0.82
	%ΔRD	− 46.97%	− 52.68%	− 60.41%	− 70.14%
	%ΔC	2.79%	24.58%	126.26%	45.81%
	ΔCSF	− 3.38	− 3.05	− 0.77	− 4.20
	LCIC	− 0.06	− 0.47	− 2.09	− 0.65
	|LCIC|	0.06	0.47	2.09	0.65
Summer	ΔRD	− 0.223	− 0.117	− 0.541	− 0.228
	ΔC	0.06	0.98	3.54	1.29
	%ΔRD	− 22.24%	− 11.68%	− 53.84%	− 22.72%
	%ΔC	3.16%	51.58%	186.32%	67.89%
	ΔCSF	− 2.26	3.88	3.68	3.41
	LCIC	− 0.14	− 4.41	− 3.46	− 2.99
	|LCIC|	0.14	4.41	3.46	2.99
Annual	ΔRD	− 0.271	− 0.298	− 0.556	− 0.404
	ΔC	0.04	0.90	2.90	1.07
	%ΔRD	− 23.31%	− 25.59%	− 47.80%	− 34.72%
	%ΔC	2.35%	53.52%	172.84%	63.64%
	ΔCSF	− 2.52	1.67	4.97	0.80
	LCIC	− 0.10	− 2.09	− 3.62	− 1.83
	|LCIC|	0.10	2.09	3.62	1.83

[a] Seasons are defined as follows: Autumn: Sept. 1–Nov. 30,015; Winter: Dec. 1, 2015–Feb. 29, 2016; Spring: Mar. 1–May 31, 2016; Summer: June 1–Aug. 31, 2016.

[b] $\Delta RD_N = RD_N - RD_1$ (N = 2, 3, 4, 5).

[c] $\Delta C_N = [DIC]_N - [DIC]_1$ (N = 2, 3, 4, 5).

[d] $\%\Delta RD_N = \Delta RD_N / RD_1$ (N = 2, 3, 4, 5).

[e] $\%\Delta C_N = \Delta[DIC]_N / [DIC]_1$ (N = 2, 3, 4, 5).

[f] $\Delta CSF = CSF_N - CSF_1$ (N = 2, 3, 4, 5).

[g] LCIC, the abbreviation for Land use Change Impact on CSF, is defined as a parameter to compare the impacts of land use change on RD and [DIC], respectively, and evaluate their combined effects on the CSF. LCIC = $\%\Delta C_N / \%\Delta RD_N$.

[h] \|LCIC\| is the absolute value of LCIC. \|LCIC\| > 1 indicates that CSF will increase because land use change-induced DIC increase dominates over RD decrease. \|LCIC\| < 1 indicates that CSF will decrease because land use change-induced RD decrease dominates over DIC increase.

Overall, there are three chief conclusions from this study. First, simulation field tests with tight control on important variables are very helpful for determining the effects of differing land use on the magnitude of carbonate weathering carbon sinks. Second, LCIC is a useful parameter to investigate the strength of the competing processes that affect carbonate weathering under different land uses. Third, in the initial stages of revegetation in karst rocky desertification areas, grass land is the optimal choice for increasing carbonate weathering-related carbon sinks.

Two main issues arising from this study need to be considered in future research. First, in this study the vegetation growth was in its initial stages. The situation is likely to change when all the types of vegetation are maturely developed; continued observation is essential, especially for the shrub land. Second, this study is performed at a small spatial scale. In future larger-scale studies, differences of input information, such as climatic conditions and complexity of land uses, need to be considered.

References

Andrews, J.A., Schlesinger, W.H., 2001. Soil CO₂ dynamics, acidification, and chemical weathering in a temperate forest with experimental CO₂ enrichment. Global Biogeochem. Cy. 15, 149–162.
Berner, R.A., 1992. Weathering, plants, and the long-term carbon cycle. Geochim. Cosmochim. Acta 56, 3225–3231.
Berner, R.A., Lasaga, A.C., Garrells, R., 1983. The carbonate-silicate geochemical cycle and its effect on atmospheric carbon dioxide over the past 100 million years. Am. J. Sci. 283, 641–683.
Broecker, W.S., Takahashi, T., Simpson, H.J., Peng, T.H., 1979. Fate of fossil fuel carbon dioxide and the global carbon budget. Science 206, 409–418.
Curl, R.L., 2012. Carbon shifted but not sequestered. Science 335, 655.
Drever, J.I., 1988. The Geochemistry of Natural Waters. 437 Prentice Hall Englewood Cliffs.
Dreybrodt, W., 1988. Processes in Karst Systems. 4 Springer.
Feely, R.A., Sabine, C.L., Lee, K., Berelson, W., Kleypas, J., Fabry, V.J., Millero, F.J., 2004. Impact of anthropogenic CO₂ on the CaCO₃ system in the oceans. Science 305, 362–366.
Gislason, S.R., Oelkers, E.H., Eiriksdottir, E.S., Sigfusson, B., Elefsen, S., Torssander, P., Kardjilov, M.I., Gisladottir, G., Snorrason, A., Hardardottir, J., 2009. Direct evidence of the feedback between climate and weathering. Earth Planet. Sci. Lett. 277, 213–222.
Hagedorn, B., Cartwright, I., 2008. Climatic and lithologic controls on the temporal and spatial variability of CO₂ consumption via chemical weathering: an example from the Australian Victorian Alps. Chem. Geol. 260, 234–253.
Houghton, R.A., Hackler, J.L., Lawrence, K.T., 1999. The U.S. carbon budget: contributions from land-use change. Science 285, 574–578.
Joos, F., 1994. Imbalance in the budget. Nature 370, 181–182.
Kump, L.R., Brantley, S.L., Arthur, M.A., 2000. Chemical weathering, atmospheric CO₂, and climate. Annu. Rev. Earth Pl. Sci. 28, 611–667.
Liu, Z., Dreybrodt, W., 1997. Dissolution kinetics of calcium carbonate minerals in H₂O-CO₂ solutions in turbulent flow: the role of diffusion boundary layer and the slow reaction H₂O + CO₂ = H⁺ + HCO₃ –. Geochim. Cosmochim. Acta 61, 2879–2889.
Liu, Z., Zhao, J., 2000. Contribution of carbonate rock weathering to the atmospheric CO₂ sink. Environ. Geol. 39, 1053–1058.
Liu, Z., Li, Q., Sun, H., Wang, J., 2007. Seasonal, diurnal and storm-scale hydrochemical variations of typical epikarst springs in subtropical karst areas of SW China: soil CO₂ and dilution effects. J. Hydrol. 337, 207–223.
Liu, Z., Dreybrodt, W., Wang, H.J., 2010. A new direction in effective accounting for the atmospheric CO₂ budget: considering the combined action of carbonate dissolution, the global water cycle and photosynthetic uptake of DIC by aquatic organisms. Earth-Sci. Rev. 99, 162–172.
Liu, Z., Dreybrodt, W., Liu, H., 2011. Atmospheric CO₂ sink: silicate weathering or carbonate weathering? Appl. Geochem. 26, S292–S294.
Liu, H., Liu, Z., Macpherson, G.L., Yang, R., Chen, B., Sun, H., 2015. Diurnal hydrochemical variations in a karst spring and two ponds, Maolan Karst Experimental Site, China: biological pump effects. J. Hydrol. 522, 407–417.
Melnikov, N.B., O'Neill, B.C., 2006. Learning about the carbon cycle from global budget data. Geophys. Res. Lett. 330, 356–360.
Parkhurst, D.L., Appelo, C.A.J., 1999. User's guide to PHREEQC (version 2) - a computer program for speciation, batch-reaction, one-dimensional transport, and inverse geochemical calculations. In: U.S. Geological Survey Water Resources Investigations Report, pp. 99–4259.
Plummer, L.N., Wigley, T.M.L., Parkhurst, D.L., 1978. The kinetics of calcite dissolution in CO₂-water systems at 5 °C to 60 °C and 0.0 to 1.0 atm CO₂. Am. J. Sci. 278, 179–216.
Raupach, M.R., Marland, G., Ciais, P., Le, Q.C., Canadell, J.G., Klepper, G., Field, C.B., 2007. Global and regional drivers of accelerating CO₂ emissions. P. Natl. Acad. Sci. 104, 10288–10293.
Raymond, P.A., Oh, N.H., Turner, R.E., Broussard, W., 2008. Anthropogenically enhanced fluxes of water and carbon from the Mississippi River. Nature 451, 449–452.
Schindler, D.W., 1999. The mysterious missing sink. Nature 398, 105–107.
Stumm, W., Morgan, J.J., 1981. Aquatic Chemistry. John Wiley & Sons, Inc., New York.
Tipper, E.T., Bickle, M.J., Galy, A., West, A.J., Pomiès, C., Chapman, H.J., 2006. The short term climatic sensitivity of carbonate and silicate weathering fluxes: insight from seasonal variations in river chemistry. Geochim. Cosmochim. Acta 70, 2737–2754.
Walker, J.C.G., Hays, P.B., Kasting, J.F., 1981. Negative feedback mechanism for the long-term stabilization of earth's surface temperature. J. Geophys. Res. 86, 9776–9782.
Yang, R., Chen, B., Liu, H., Liu, Z., Yan, H., 2015. Carbon sequestration and decreased CO₂ emission caused by terrestrial aquatic photosynthesis: insights from diel hydrochemical variations in an epikarst spring and two spring-fed ponds in different seasons. Appl. Geochem. 63, 248–260.

Yang, M., Liu, Z., Sun, H., Yang, R., Chen, B., 2016. Organic carbon source tracing and DIC fertilization effect in the Pearl River: insights from lipid biomarker and geochemical analysis. Appl. Geochem. 73, 132–141.

Zeng, C., Liu, Z., Yang, J., Yang, R., 2015a. A groundwater conceptual model and karst-related carbon sink for a glacierized alpine karst aquifer, Southwestern China. J. Hydrol. 529, 120–133.

Zeng, C., Liu, Z., Zhao, M., Yang, R., 2015b. Hydrologically-driven variations in the karst-related carbon sink fluxes: insights from high-resolution monitoring of three karst catchments in Southwest China. J. Hydrol. 533, 74–90.

Zhao, M., Zeng, C., Liu, Z.H., Wang, S.J., 2010. Effect of different land use/land cover on karst hydrogeochemistry: a paired catchment study of Chenqi and Dengzhanhe, Puding, Guizhou, SW China. J. Hydrol. 388, 121–130.

Zhu, H., Zeng, C., Liu, Z.H., Zeng, Q.R., Li, L.L., 2015. Karst-related carbon sink flux variations caused by land use changes: an example from the Puding karst test site in Guizhou. Hydrol. Eng. Geol. 42, 120–125 (In Chinese with an English Abstract).